Structural and nuclear characterizations of defects created by noble gas implantation in silicon oxide

H. Assaf, E. Ntsoenzok, M.-F. Barthe, M.-O. Ruault, T. Sauvage, S. Ashok

▶ **To cite this version:**

H. Assaf, E. Ntsoenzok, M.-F. Barthe, M.-O. Ruault, T. Sauvage, et al.. Structural and nuclear characterizations of defects created by noble gas implantation in silicon oxide. E-MRS IUMRS ICEM 2006 Spring Meeting - Symposium U: Si-based Materials for Advanced Microelectronic Devices: Synthesis, Defects and Diffusion, May 2006, Nice, France. pp.222-226, 10.1016/j.nimb.2006.10.042 . in2p3-00115973

HAL Id: in2p3-00115973
https://hal.in2p3.fr/in2p3-00115973

Submitted on 24 Nov 2006

HAL is a multi-disciplinary open access archive for the deposit and dissemination of scientific research documents, whether they are published or not. The documents may come from teaching and research institutions in France or abroad, or from public or private research centers.

L'archive ouverte pluridisciplinaire **HAL**, est destinée au dépôt et à la diffusion de documents scientifiques de niveau recherche, publiés ou non, émanant des établissements d'enseignement et de recherche français ou étrangers, des laboratoires publics ou privés.

Structural and nuclear characterizations of defects created by noble gas implantation in silicon oxide

H. Assaf[1], E. Ntsoenzok[1,2], M.-F. Barthe[1], M.-O. Ruault[3], T. Sauvage[1], S. Ashok[4].
[1]CERI-CNRS, 3A, rue de la Férollerie, 45071 Orléans, France.
[2]LESI, University of Orleans, 21 rue de Loigny la bataille, 28000 Chartres, France
[3]CSNSM, CNRS-IN2P3, Batiment 108-F-91405 Orsay, France.
[4]Department of Engineering Science, the Pennsylvania State University, 212 Earth and Engineering Science Building, University Park, PA 16802, USA.

Abstract

Thermally grown silicon oxide layer was implanted at room temperature with 300keV Xe at fluences ranging from 0.5 to $5x10^{16}Xe/cm^2$. Bubbles created after Xe-implantation provided a low-k silicon oxide that has potential use as a dielectric material for interconnects in Si integrated circuits. Transmission Electron Microscopy (TEM), Rutherford Backscattering Spectrometry (RBS) and Positron Annihilation Spectroscopy (PAS) were used to provide a comprehensive characterization of defects (bubbles, vacancy, gas atoms and other types of defects) created by Xe implantation in SiO_2 layer. These measurements suggest that the bubbles observed with TEM for all fluences were a consequence of the interaction between Xe and vacancies (V), with V_nXe_m complexes created in the zone where V and Xe profiles overlap. Negatively charged defects such as ($Si\text{-}O^-$, $Si\text{-}O\text{-}O^-$ and O_2^-) are also created after implantation.

Introduction

The speed of ULSI circuits is becoming dominated less by the speed of the individual devices but more by the RC time constant of the layers of interconnects tying the devices together[1]. To date SiO_2 has been the dielectric material of choice in this application, but because of its relatively high permittivity (k ~ 4), it contributes to a large capacitance between the metal layers and thus a large RC delay to the circuit[2]. By reducing the permittivity of SiO_2, the RC delay might be reduced leading to faster performances[3]. The implantation of heavy noble gas such as Xe in silicon oxide was recently used for decreasing its permittivity and thus offering prospects for a new technique to produce an ultra low-k dielectric (ULK) with $k \leq 1.5$[4,5]. This k reduction is due to the bubble formation in the silicon oxide. No model has yet been proposed to study the formation and growth mechanisms of bubbles in SiO_2 matrix, while these mechanisms are quite well known in metals[6] and semiconductors[7].

This paper deals with an extensive characterization of defects (vacancy or negatively charged defects, bubbles and gas atoms) induced by Xe-implantation in silicon oxide. For this purpose, TEM, RBS and PAS techniques were used.

Experimental procedure

A 2.3µm silicon oxide was grown by heating n-type silicon wafers at 1100°C in air. Some of these SiO_2/Si structures were implanted, at room temperature, by 300keV Xe at various fluences: 0.5, 1, 3.5 and $5 \times 10^{16}/cm^2$. Such an energy results in Xe implantation at a depth of 125nm as simulated by TRIM. Bubble formation after Xe implantation in silicon oxide was characterized by cross-sectional transmission electron microscopy (XTEM) using a Philips CM12 microscope.

Rutherford backscattering spectrometry (RBS) was used to obtain the Xe distribution in silicon oxide. RBS measurements were performed using a 2MeV ^{4}He beam provided by a 3.5MeV Van de Graaff accelerator.

Positron annihilation spectroscopy (PAS) was performed in order to study the defects induced by Xe-implantation using a monoenergetic positron beam with energies tuneable over 0.5-25keV[8]. In this energy range, the positron mean implantation depth in SiO_2 calculated by using the equation $Z(E)\ [nm] = 12.75 \times E^{1.7}[keV]$ with the same parameters as for Si[9] varies from 40 to 3000 nm. After implantation and thermalization, positron diffuses through the solid until it either annihilates with an electron in a delocalized state or is trapped at a defect. Free annihilation results in the emission of two 511 keV $\pm$ ΔE photons where ΔE is proportional to the momentum of the electron-positron annihilated pairs (Doppler broadening). The two-photon annihilation events are detected at room temperature with a Ge detector. Approximately 10^6 events were collected in the peak at each positron energy value. The various annihilation processes can be distinguished by analyzing the shape of the photo-peak. The shape is defined by the S(hape) and W(ing) parameters. The S parameter is defined as the relative contribution of the central part of the peak in the energy window 511[-0.66;+0.66] keV and is the fraction of annihilation with low momentum electrons, mainly the valence electrons. The W parameter is defined by the relative contributions in the wings of the peak in the energy windows 511[-6.64;-2.57] keV and 511[+2.57;+6.64] keV and is the fraction of annihilation with high momentum electrons, mainly the core electrons. The S and W distribution as a function of depth are determined by the consistent fitting of the S(E) and W(E) data measured as a function of positron energy using a modified version of the VEPFIT program[10]. The sample is modelled as a sequence of n homogeneous layers with the annihilation characteristics S_i, W_i and the positron effective diffusion length L_i^+ specific to the layer i. In our case, S(E) and W(E) evolutions are fitted for energy higher than 1.5 keV. The

data below 1.5 keV are discarded because in this range the positrons migration is not only due to a diffusion process.

Results and discussion

Fig.1-a presents the typical XTEM images obtained in 2.3µm silicon oxide by 300keV Xe ion implantation at different fluences: 0.5, 1, 3.5, and $5x10^{16}/cm^2$. Extended defects can be observed and they can be attributed to bubbles/cavities induced in SiO_2 by implantation. Their size distributions show that for the sample implanted at 0.5 and $1x10^{16}/cm^2$ fluences the majority of bubbles has a mean diameter less than 6nm. The mean diameter increases with the fluence. At 3.5 and $5x10^{16}/cm^2$, bubbles present a wider range of diameters - from ~6nm up to 40nm. The thickness of the bubble/cavity band increases with the implanted fluence from 65nm for the lowest fluence ($0.5x10^{16}Xe/cm^2$) to 160nm for the highest one ($5x10^{16}Xe/cm^2$). Fig.2-a illustrates the evolution of Xe profiles with the Xe fluence in silicon oxide as measured by RBS technique. For the fluences of 0.5 and $1x10^{16}Xe/cm^2$, the Xe distribution has a gaussian profile centered at 116nm depth while for the higher fluences of 3.5 and $5x10^{16}Xe/cm^2$, Xe profiles consist of a main peak with two shoulders on both sides. The main peak is located at the depth of 95 and 90nm for the fluence of 3.5 and $5x10^{16}Xe/cm^2$ respectively. The region where Xe is detected corresponds to the largest bubble zone. It suggests that Xe is predominantly located inside the bubbles. According to TRIM simulations, displacement per atom (dpa) [called also “vacancy” (V) if the displaced atom does not return to its initial position after implantation] and Xe peaks are located at depths of 85nm and 125nm respectively, as shown in Fig. 2-b. We can then conclude that bubbles are formed between these two zones, probably in the zone of overlapping of V and Xe where the most stable V_nXe_m complexes are created. Since, the fluence is very large, overlapping is expected as seen in fig.2-b.

In fig. 3, the low and high momentum annihilation fractions S and W values are plotted as a function of the positron implantation energy E (S(E) and W(E)) for the SiO_2/Si structures before and after Xe implantation. Before implantation (reference sample), S(E) increases with positron energy first rapidly up to 5keV where it reaches a plateau value at about 15keV and then S(E) increases again more slightly up to 25keV. W(E) has the reversible evolution of S(E) but from the energy of 15keV, its decrease is more significant than the increase of S(E). Using the VEPFIT program, the evolution of S(E) and W(E) can be fitted with a model of two homogeneous layers: Layer 1 the virgin SiO_2 layer with the annihilation characteristics (S_{SiO2}~0,471(1), W_{SiO2}~0,0491(1)) and layer 2 the virgin silicon substrate with the annihilation characteristics (S_{Si}~0,472(1), W_{Si}~0,0275 (1)). The effective diffusion length (L^+) of positrons is about 36 nm for SiO_2 (layer 1) and 230 nm for Si (layer 2). L^+ is short in the SiO_2 layer, indicating that positrons are trapped in this virgin SiO_2 layer.

After Xe-implantation, S(E) decreases in the region of positron energy between 0.5 and 5/6keV depending on the implanted fluence. At this energy, the mean implantation depth of positrons is about 270nm. W(E) has the reverse behaviour. Then S(E) increases (and W(E) decreases) with positron implantation energy up to 25keV, regardless of the implanted fluence. Using VEPFIT program, S(E) and W(E) curves can be fitted with a mode describing the sample as four homogenous layers. From the surface positron probe, first two are damaged SiO_2 layers (1 and 2) and then the third and fourth layers correspond respectively to the undamaged SiO_2 layer and Si substrate. The (S,W) values obtained for the layer 3 and 4 are equal to the annihilation characteristics of the virgin SiO_2 (S_{SiO2} ,W_{SiO2}) and of the Si substrate (S_{Si},W_{Si}), respectively, irrespective of the implanted fluences. Parameters characterizing the damaged SiO_2 (layers 1 and 2) are shown in the Table I. The S_1 low momentum fraction increases (as W_1 high momentum fraction decreases) in layer 1 and S_2 decreases (W_2 increases) in layer 2 when the fluence increases. The values of S_1 and S_2

determined in the two damaged (layers 1 and 2) remain lower than S_{SiO2} and the values of W_1 and W_2 are largely higher than $W_{SiO2,}$ whatever the implanted fluence. It indicates that the nature or the distribution of the annihilation states detected by the positrons change after implantations in the layers 1 and 2. The effective diffusion length of positron (L^+) is shorter than the value obtained in the virgin SiO_2 layer, highlighting the existence of defects which trap positron and limit their diffusion into the SiO_2 up to the surface. Two types of point defects have already been identified (see references for details)[11] to be created in silicon oxide. Some of these defects can trap positrons leading to the S and L^+ evolution as presented in Table II. When the defect is an open-volume type like the vacancy, S is expected to increase. In these SiO_2 layers, Si and O atoms can be displaced during implantation, leading to the formation of different vacancy defects like oxygen, or silicon monovacancies or defects with larger open volume. As reported by Richard et al[12], the stable vacancy defect created by implantation in SiO_2 is the neutral oxygen vacancies due to its very low formation energy; the Si-vacancy is not very stable after implantation. It suggests that positrons could be trapped in these neutral oxygen vacancies or in defects with larger open volume leading to the increase of the low momentum fraction S after implantation. The S decrease is expected when positrons are trapped at acceptor and non vacancy-like defects that can be assimilated to "negative ions" such as O_2^- (dissolved oxygen molecules), $\equiv Si-O^-$ (NBOHC centers), $\equiv Si-O-O^-$ (POR centers))[13, 14]. According to our PAS results, we can conclude that the dominant defects detected after Xe-implantation in silicon oxide are the "negative ions". We cannot specify exactly which defect (dissolved oxygen molecules, NBOHC or POR centers) leads to the reduction of S and L^+. Fujinami et al[13] proposed that "NBOHC centers" trap positrons in boron-implanted SiO_2, while Knights et al[14] concluded from detailed detection by using EPR and PAS techniques that dissolved oxygen, NBOHC or POR centers could be the defects leading to the S decrease in SiO_2 implanted with Ge ions.

In Xe implanted samples we have observed that S_1 values determined in layer 1 are higher than the ones obtained in layer 2; moreover S_1 increases when implantation fluence increases (see Table I). This suggests that, in this layer, vacancy-defects (oxygen vacancies or defects with larger open volume) also exist and their concentration or their size increases with the fluence. The thickness of this layer 1 depends on the Xe fluence - it is 140 nm for the lowest fluence and increases to 200nm for the highest.

Comparing PAS results with TEM and RBS results, we can conclude that layer(1) corresponds to the bubble region where the Xe has maximum concentration. In this layer, vacancies (V_n, detected by PAS) can interact with Xe atoms (detected by RBS) and create the V_nXe_m complexes that are visible in XTEM images as bubbles. The layer 2 is located deeper than the layer 1. In this layer S decreases slightly with the Xe fluence, suggesting that the concentration of the negatively charged defects increases with the fluence. The maximum width of defect layer is larger than the one calculated by TRIM (approximately 230 nm), and ranges from 360nm for the lowest fluence and >385nm for the highest fluence. Layer2 is located deeper than the implanted region projected by TRIM, hence we suggest that the negatively charged defects detected in this layer are more probably formed by ejection of interstitial oxygen from the implanted region (layer1) to layer2. Interstitial oxygen atoms ejected in this layer can exist as dissolved oxygen molecules (O_2^-) or if they have a sufficient energy, they can break Si-O-Si bonds in the matrix and form NBOHC and POR centers deeper than the Xe range.

Summary

The following major results can be underlined:

- Xe implantation in SiO_2 induces bubbles whose size and distribution evolve with the Xe fluence.

- Xe distribution in silicon oxide is fluence-dependent. A gaussian profile is obtained for the lowest fluences (0.5 and $1x10^{16}Xe/cm^2$) while for the highest fluences (3.5 and $5x10^{16}Xe/cm^2$) a main peak with two shoulders on both sides is observed.
- Positron Annihilation Spectroscopy (PAS) shows that the dominant defects detected in silicon oxide after implantation are the negatively charged defects (O_2^-, and/ or NBOHC and/or POR centers). These defects are formed in the whole of implanted region and detected at depths greater than 385nm.
- Vacancy defects (oxygen vacancies or defects with large open volume) were also detected by PAS technique. These defects are localized in the bubble region as observed by TEM. The concentration and the size of these defects increases with the implanted fluence. In this region, RBS results shows that the concentration of Xe atoms is maximum, suggesting that interactions of the Xe atoms and vacancies in this region lead to the formation of Xe_nV_m complexes that can be the precursors to the bubbles.

References

1- International Technology Roadmap for Semiconductors 2003, Semiconductor Industry Association, www.itrs.net.

2- J. Xu, J. Moxom, S. Yang, and R. Suzuki, T. Ohdaira, Appl. Surf. Sci. **194**, (2002), 189.

3- Z.-C. Wu, Z.W. Shiung, C.C. Chiang, W.H. Wu, M.C. Chen, S.M. Jeng, W. Chang, P.F. Chou, S.M. Jang, C.H. Yu, M.S. Liang, J. Electrochem. Soc. **148,** (2002),115.

4- H. Assaf, E. Ntsoenzok, M. -O. Ruault, O. Kaitasov, Solid State Phenom. **108/109**, (2005), 291.

5- E. Ntsoenzok, H. Assaf, M.-O. Ruault, Semiconductor Defect Engineering – Materials, Synthetic Structures and Devices, MRS Vol. **864**, San Francisco, CA, edited by S. Ashok, J. Chevallier, B.L. Sopori, M. Tabe and P. Kiesel (Materials Research Society, Warrendale, PA) (2006), p. 327.

6- C.H. Zhang , K.Q. Chen, Y.S. Wang, J.G. Sun, D.Y. Shen, Journal of Nuclear Materials **245**, (1997), 210.

7- S. Godey, T. Sauvage, E. Ntsoenzok, H. Erramli, M.F. Beaufort, J.F. Barbot, B. Leroy, J. Appl. Phys. **87**, (1999), 2158.

8- P. Desgardin, L. Liszkay, M-F Barthe, L. Henry, J. Briaud, M. Saillard, L. Lepolotec, C. Corbel, G. Blondiaux, A. Colder, P. Marie and M. Levalois, Materials Science Forum **363-365**, (2001), 523.

9- A. Van Veen, H. Schut, J. De Vries, R.A. Hakvoort, and M.R. Ijpma, AIP Conf. Proc. **218**, (1990), 171.

10- E. Soininen, J. Mäkinen, D. Beyer and P. Hautojärvi, Phys. Rev. B **46**, (1992), 13104.

11- C.H. de Novin, A. Barbu, Solid State Phenom. **30& 31**, (1993), 227.

12- N. Richard, L. Martin-Samos, G. Roma, Y. Limoge, J-P. Crocombette, J. of Non-crystalline Solids, **351**, (2005), 1825.

13- M. Fujinami, N.B. Chilton, Appl. Phys; Lett. **62**, (1993), 1131.

14- A.P. Knights, L.B. Allard, J.L. Brebner, P.J. Simpson, Nucl. Instr. and Meth. **B 127-128**, (1997), 86.

	Fluences (Xe/cm^2)	**$5x10^{15}$**	**$1x10^{16}$**	**$3,5x10^{16}$**	**$5x10^{16}$**
layer (1)	thickness (nm)	140(3)	149(3)	192(5)	200(5)
	S	0.429(0.8)	0.431(1)	0.442(1)	0.449(1)
	W	0,0572(1)	0,0564(0.6)	0,0528(1)	0.0505(1)
	L^+ (nm)	7(1)	3(0.5)	2.5 (0.5)	2.5(0.5)
layer (2)	thickness (nm)	220(1)	211(1)	184(1)	185(1)
	S	0.409(1)	0,408(1)	0,405(1)	0,403(1)
	W	0.0619(1)	0.0621(1)	0.0628(1)	0.0632(1)
	L^+(nm)	9(1)	9(1)	9(1)	9(1)

TableI: Positron annihilation parameters (S, W and L^+) and thickness of damaged layers formed after Xe implantation with different fluences in silicon oxide layer as determined by fitting the S(E) and W(E) curves with a model of homogeneous layers using a modified version of VEPFIT[10].

name	structures	Evolution of positron characteristics
vacancy defects	$\equiv Si - Si \equiv$ and ≡Si-O-O-Si≡	S↗, W↘, L^+↘
Dissolved oxygen	O_2^-	S↘, W↗, L^+↘
E' centers	$\equiv Si^+$	-
NBOHC centers	$\equiv Si - O^-$	S↘, W↗, L^+↘
Peroxy radical	$\equiv Si - O - O^-$	S↘, W↗, L^+↘

TableII: Defects created in silicon oxide after implantation from published literature and expected evolution of the characteristics of the positrons S, W and L^+ when they are trapped by these defects .

Figure captions

Figure 1: XTEM images of silicon oxide layers implanted with 300keV Xe at different fluences: $0.5x10^{16}Xe/cm^2$, $1x10^{16}$ Xe/cm^2, $3.5x10^{16}$ Xe/cm^2 and $5x10^{16}$ Xe/cm^2.

Figure 2: (a) Evolution of Xe depth profiles obtained by RBS in SiO_2 implanted with Xe at different fluences and (b) displacement per atom (dpa) and Xe depth profiles in SiO_2 implanted with 300keV Xe at $5x10^{16}Xe/cm^2$ as calculated by using TRIM program.

Figure 3: Evolution of the low and high momentum annihilation fractions (S, W) as a function of positron implantation energy in SiO_2/Si structures before and after Xe implantation at different fluences : $0.5x10^{16}Xe/cm^2$, $1x10^{16}$ Xe/cm^2, $3.5x10^{16}$ Xe/cm^2 and $5x10^{16}$ Xe/cm^2. The solids lines are a fit of the (S, W) curves with a model of homogeneous layers using a modified version of VEPFIT[10]. The mean implantation depth in SiO_2 is calculated as z(E) [nm] $=12.75 \times E^{1.7}$ [keV][9].

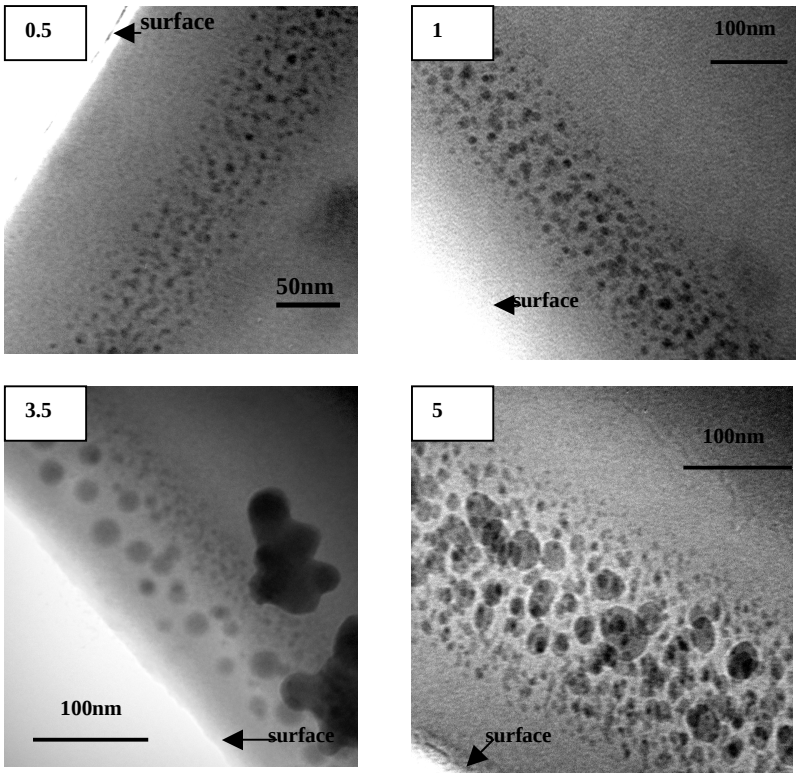
0.5
surface
50nm
1
100nm
surface
3.5
100nm
surface
5
100nm
surface

FIG.1

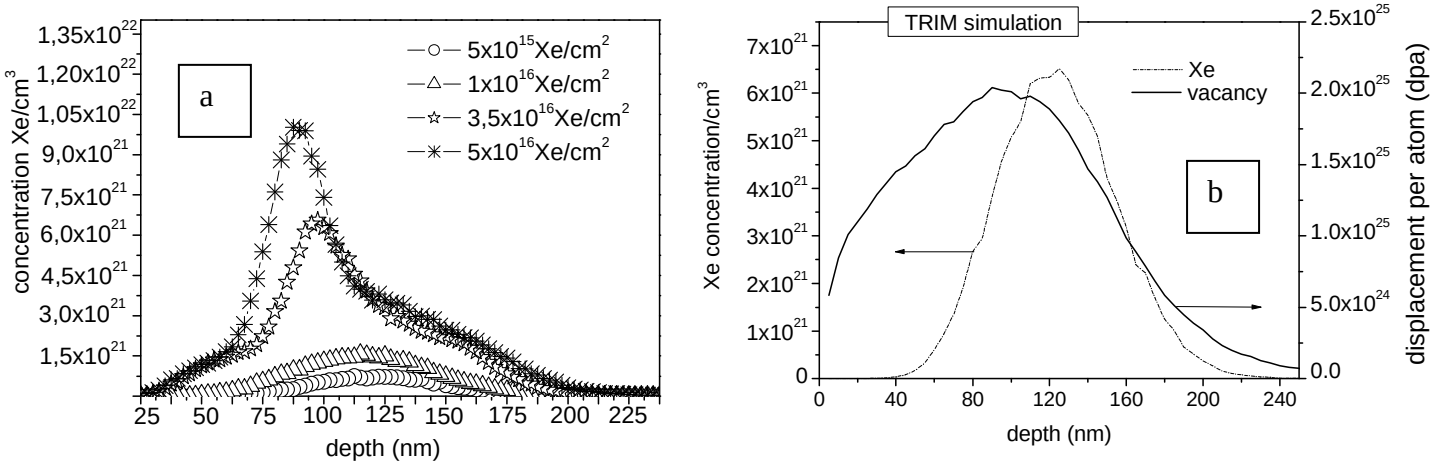
a
5x10^15Xe/cm^2
1x10^16Xe/cm^2
3,5x10^16Xe/cm^2
5x10^16Xe/cm^2
concentration Xe/cm^3
depth (nm)
TRIM simulation
Xe
vacancy
b
Xe concentration/cm^3
displacement per atom (dpa)
depth (nm)

FIG.2

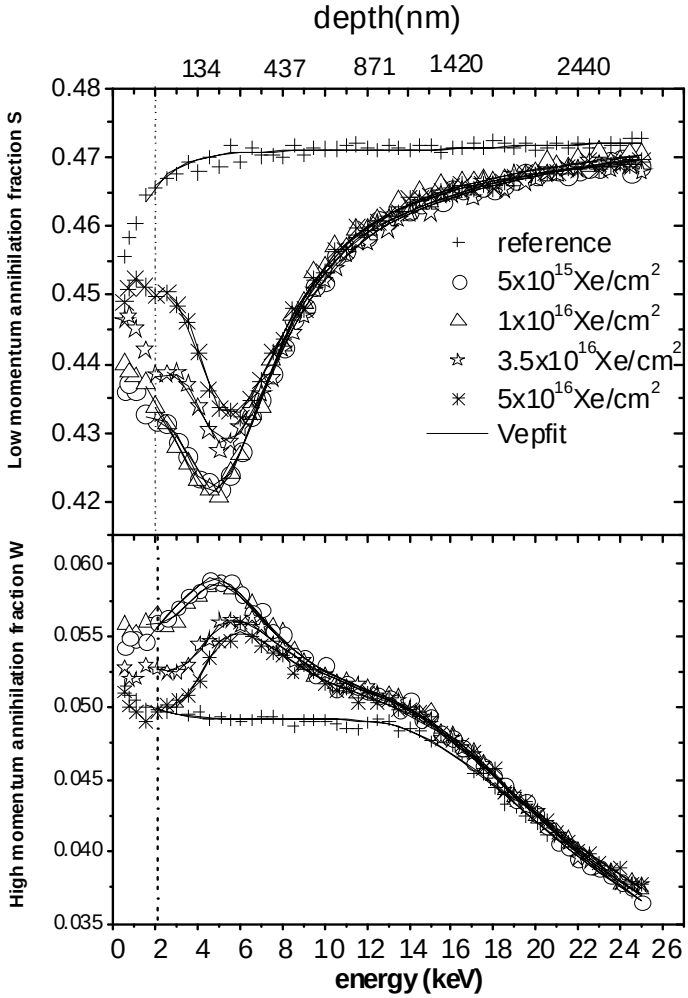
depth(nm)
134
437
871
1420
2440
Low momentum annihilation fraction S
High momentum annihilation fraction W
reference
5x10^15 Xe/cm^2
1x10^16 Xe/cm^2
3.5x10^16 Xe/cm^2
5x10^16 Xe/cm^2
Vepfit
energy (keV)

FIG.3